Efficient Full-Wave Method of Moments Analysis and Design Methodology for Radial Line Planar Antennas

Oleg Becker, *Student Member, IEEE*, and Reuven Shavit, *Senior Member, IEEE*

***Abstract*—An efficient full-wave MoM analysis and a design methodology for radial line planar antennas (RLPA) is presented. The feeding network of the antenna is solved by using the appropriate Green's function defined for the problem. Filling of the Z-matrices is considerably simplified due to the analytical formulation of the MoM. Also, assumptions made on the minimum size of the coupling neighborhood for the feeding conductive probes in the radial line enabled significant time reduction of the time spent on the matrix inversion. Moreover, exploration of the RLPA symmetries leads to several improvements in the overall performance. The MoM results of the feeding network are combined with the results of the radiating elements for obtaining the performance of the feeding network under load conditions. It is shown that the radial position of the radiating elements in the RLPA resemble an equilateral triangular array grid. This observation enabled to perform the analysis of the array external mutual coupling effect using the equivalent "unit-cell" concept derived from an infinite phased array analysis. Comparison of the MoM results of the feeding network to CST commercial software show significant computational timesavings and the results are found to be in a good agreement.**

***Index Terms*—Method of moments (MoM), radial line planar antenna (RLPA).**

I. Introduction

THE increased demand for higher transmission capacity is driving the research to investigate new ways to operate in multiple frequencies with orthogonal polarizations. This requirement motivated the current research to look for a high gain, dual frequency and dual circular polarization antenna for two-way Ku-band satellite communication. Although microstrip array antennas are an attractive candidate in view of their cost, weight and low profile, they encounter difficulties in achieving high gain values in excess of 30 dBi. The main reason resides in conduction and dielectric losses due to the large length of the microstrip transmission lines forming the feeding network. In order to overcome the problem associated with high conduction losses but remain with microstrip radiating elements, an alternative feeding structure in the form of a radial line has been proposed for planar antennas. A radial line power distribution network was first conceptualized and built by Goebels and Kelly [1] to feed an antenna with annular slots as radiators, also called radial line slot antenna (RLSA). The authors provided a general approach to get an arbitrary polarization from the radiating slots by their proper orientation on the radial line top surface. A derivative from RLSA concept was studied by Carver [2] and Nakano [3]. They used low profile helices fed from a radial line through small conductive probes to obtain circular polarization. The radial line was excited at its center by a probe and the helices were distributed on concentric circles on the top surface of the radial line. In 1991, Haneishi *et al.* [4] replaced the helices with circular polarized microstrip elements to obtain a Ku band radial line planar antenna (RLPA) with high efficiency (90%). The same concept and radiating elements were used also by Yamamoto *et al.* [5] to design an RLPA with shaped beam.

One of the main issues in the RLPA design is the proper selection of the feeding probes lengths in the radial line. This selection directly affects the antenna amplitude distribution and thus the overall antenna performance. Various attempts to perform the analysis of the radial line-feeding network can be found in the literature. In [6], [7] closed-form expressions for the self and mutual impedances were computed using the electromotive force (EMF) method making the assumption of a single term cosine current distribution on the probes. An additional assumption made is that all probes are equally matched with a constant termination Z_0 neglecting the coupling between radiators outside the radial line. In [8]–[10] Pazin and Leviatan suggested a synthesis procedure for the feeding network that uses an approximate model of monopoles in free space to simulate the feeding probes in the radial line and takes into account the mutual coupling from neighboring probes according to the same model. This procedure was used in [11], [12] to design a new type of Ku-band, dual frequency and dual circular polarization multilayer microstrip array antenna with low side-lobes fed from a radial line through conductive probes. All these analyses have limited accuracy and result in unsatisfactory comparison between the required performance of the antenna (side lobe level, aperture efficiency, and matching) and the actual measured results. An improved and more accurate analysis approach is described in [13] using a mode matching analysis on each discontinuity (antenna probe) in order to find the equivalent circuit for the radial line loaded with the antenna's probes. The analysis assumes a rotational symmetry of the system. However, it is impossible to apply this model to applications with scattering that breaks this symmetry [11]. Recently in [14], it has been reported on full wave analysis using the method of moments (MoM) for the analysis of the RLSA. The major drawback of full wave analysis of the RLPA, which takes in consideration the internal

Manuscript received June 20, 2010; revised October 12, 2010; accepted November 25, 2010. Date of publication April 19, 2011; date of current version June 02, 2011.

The authors are with the Department of Electrical and Computer Engineering, Ben Gurion University of the Negev, Beer-Sheva 84105, Israel (e-mail: olegb@ee.bgu.ac.il; rshavit@ee.bgu.ac.il).

Color versions of one or more of the figures in this paper are available online at http://ieeexplore.ieee.org.

Digital Object Identifier 10.1109/TAP.2011.2143687

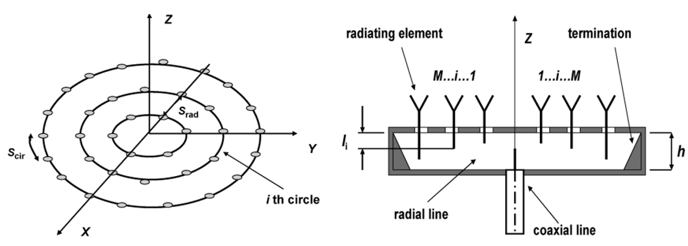

Fig. 1. The geometry of the radial line (a) element layout (b) radial line side view.

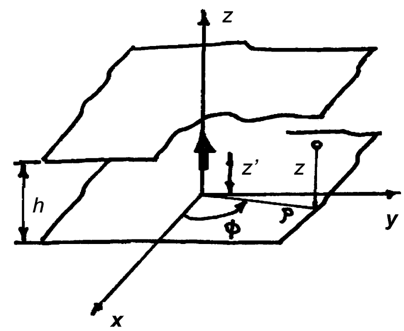

Fig. 2. The geometry of a z directed elementary current between two parallel plates.

coupling between the feeding probes and the external coupling between the radiating elements, is its numerical and computational complexity, especially for large arrays with hundreds of elements, which makes it prohibitive for a design and optimization process.

The general geometry of the RLPA is shown in Fig. 1. The antenna consists of a radial line with a central excitation probe and probe-fed radiating elements. The inter element spacing between elements is S_{cir}, the distance between the circles is S_{rad}, the height of the radial line is h and the probe lengths in the nth circle *is* l_n.

The radial line is made of perfect electrical conductor (PEC) and filled with air. The excitation probe is simply an extension of the central probe of the coaxial feeding line that protrudes into the radial line. An outward traveling wave excited by the central probe couples the electromagnetic energy to the radiating elements feeding probes. The height dimension of the radial waveguide is selected to support only the dominant transverse electromagnetic mode (TEM) and the other, higher modes are evanescent. The number of the radiating elements determines the diameter of the parallel plate waveguide. The radial line is terminated with an absorbing material evenly distributed on its perimeter. In this case, a non-resonant structure with a traveling wave nature is obtained. Alternatively, the antenna rim can be short circuited with a PEC to obtain a resonant structure in the radial line. In this case, a higher (close to 100%) radiation efficiency can be obtained, but the Green's functions required are more involved. The array of radiating elements is made of N identical radiators fed by probes. They are located on concentric circles with $6n$ elements in circle number n. Such placement ensures a more efficient coverage of the radial waveguide top surface [2].

In this paper, an efficient MoM formulation and a numerical methodology based on the full wave analysis of the structure of the radial line feeding network is presented. This procedure can be used in an optimization design process of the RLPA taking in consideration both the internal and the external coupling between the radiating elements. In the proposed analysis, the appropriate Green's functions for a non-resonant structure are derived and the induced currents on the feeding conductive probes are found using an efficient MoM procedure.

In Section II, the Green's functions used in the problem formulation are introduced and the process of the integration of the feeding network with the radiating element is explained. In Section III the design methodology is explained and in Section IV, a numerical example for the design of 7-circles RLPA is given and the results are compared to the CST software. Finally, in Section V some conclusions are drawn.

II. Theory

A. Green's Functions Formulation

Three different dyadic Green's functions are required for the solution of the feeding network shown in Fig. 1. The first dyadic Green's function is related to the currents flowing in the z-direction on the probe surface. The second dyadic Green's function is related to the excitation region at the base of the probe, which can be represented by an equivalent magnetic current ring. The third dyadic Green's function is added due to radial currents, which develop on the cap of each probe. Adding this function allows us to get results that are more precise in long probes cases, which are in close proximity to one of the PEC plates of the RLPA.

The geometry for the first dyadic Green's function is shown in Fig. 2.

The parallel plates are made of PEC and separated by the distance h. The magnetic vector potential, $\underline{A}$ due to the electrical current source, $\underline{J}(z')$ in the parallel plate structure can be written in the form,

$$\underline{A} = \mu \int_{s'} \underline{\underline{G}}(\rho, z; z')\, \underline{J}(z') ds' \tag{1}$$

in which $\underline{\underline{G}}(\rho, z; z')$ is the dyadic Green's function for an electrical current source positioned at coordinate $(0, 0, z')$ and μ is the medium permeability. The conductive probe has a radius a and length l carrying a current distribution, $J_z(z')$. Rotational symmetry is assumed during the solution of the problem so we have $\partial/\partial\phi = 0$. Solution of the problem in cylindrical coordinates for the z-directed magnetic vector potential yields the $\hat{z}\hat{z}$ dyadic Green's function component,

$$\begin{aligned} &G_{zz}(\rho, z, z') \\ &\quad = \frac{1}{4jh} \sum_{n=0}^{\infty} \varepsilon_n \cos\left(\frac{\pi n}{h} z'\right) \cos\left(\frac{\pi n}{h} z\right) H_0^{(2)}(k_\rho \rho) \end{aligned} \tag{2}$$

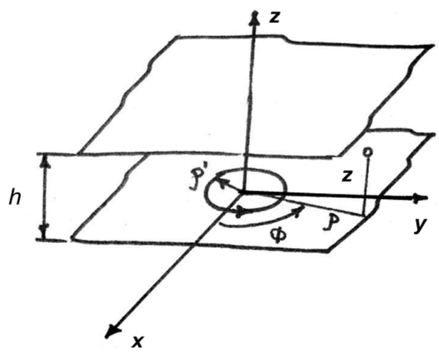

Fig. 3. The geometry of an annular magnetic current between two parallel plates.

with $\varepsilon_n = \begin{cases} 1, & n=0 \\ 2, & n \geq 1 \end{cases}$ and $k_\rho = \sqrt{k^2 - (\pi n/h)^2} \cdot H_0^{(2)}(k_\rho \rho)$ is the Hankel function of second kind and zero order [15].

Knowledge of the z directed magnetic vector potential enables to compute the electric fields E_z, $E\rho$ and the magnetic field $H\phi$ in the parallel plates as described in [17].

The geometry for evaluating the second dyadic Green's function is shown in Fig. 3.

The excitation describes the radial electric field in the coaxial opening of the exciting central probe of the parallel plate structure. The radial electric field can be represented by an equivalent annular magnetic current source. The magnetic field, $\underline{H}$ due to this magnetic current source, $\underline{J}_m(\rho')$ can be written in the form,

$$\underline{H} = -j\omega\varepsilon \int_{s'} \underline{\underline{G}}(\rho, z; \rho', z') \underline{J}_m(\rho') ds' \tag{3}$$

in which $\underline{\underline{G}}(\rho, z; \rho', z')$ is the dyadic Green's function and ϵ is the medium permittivity. Rotational symmetry is assumed so we have $\partial/\partial\phi = 0$. Solution of the problem in cylindrical coordinates for the ϕ directed magnetic field [16] for an annular magnetic current source of radius ρ' placed at $(0,0,z')$ yields the $\widehat{\phi}\widehat{\phi}$ dyadic Green's function component,

$$\begin{aligned} G_{\phi\phi} = &-\frac{j\pi\rho'}{2h} \sum_{n=0}^{\infty} \varepsilon_n \cos\left(\frac{\pi n}{h} z'\right) \\ &\times \cos\left(\frac{\pi n}{h} z\right) \begin{cases} H_1^{(2)}(k_\rho \rho') J_1(k_\rho \rho) & \rho \leq \rho' \\ J_1(k_\rho \rho') H_1^{(2)}(k_\rho \rho) & \rho \geq \rho' \end{cases} \end{aligned} \tag{4}$$

in which $H_1^{(2)}(k_\rho \rho)$ is the Hankel function of second kind and first order and $J_1(k_\rho \rho)$ is the Bessel function of first order [15]. Knowledge of H_ϕ magnetic field enables to compute the electric fields E_z, $E\rho$ in the parallel plates as described in [17].

The third dyadic Green's function is due to radial currents, which develop on the cap of the conductive probes with radius a. This consideration is significant for long probes cases in which the probes caps become strongly coupled to the closest PEC plate of the radial line. This capacitive coupling need to be taken in consideration to improve the accuracy of the computations as will be shown in the following. The geometry for the third dyadic Green's function is shown in Fig. 4.

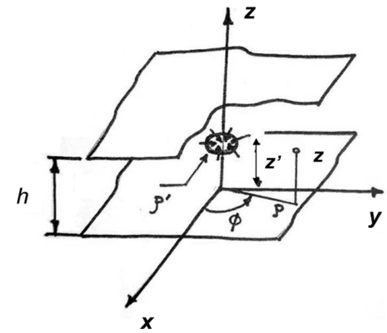

Fig. 4. The geometry of an annular radial current between two parallel plates.

The magnetic field, $\underline{H}$ due to these radial electric current sources, $\underline{J}(\rho')$ can be written in the form,

$$\underline{H} = \int_{s'} \underline{\underline{G}}(\rho, z; \rho', z') \underline{J}(\rho') ds' \tag{5}$$

in which $\underline{\underline{G}}(\rho, z; \rho', z')$ is the dyadic Green's function. Due to the rotational symmetry of the problem we assume $\partial/\partial\phi = 0$.

Solution of the problem in cylindrical coordinates for the ϕ directed magnetic field [16] for a radial directed annular current source of radius ρ' placed at $(0,0,z')$ yields the $\widehat{\phi}\widehat{\rho}$ dyadic Green's function component,

$$\frac{\partial}{\partial\rho}\frac{1}{\rho}\frac{\partial}{\partial\rho}(\rho G_{\phi\rho}) + \frac{\partial^2 G_{\phi\rho}}{\partial z^2} + k^2 G_{\phi\rho} = -\delta(\rho - \rho')\delta'(z - z') \tag{6}$$

with the boundary conditions $\partial G_{\phi\rho}/\partial Z = 0$ at $z = 0, h$. Use of the separation of variables method results in

$$\begin{aligned} G_{\phi\rho} = &-\frac{j\pi^2\rho'}{h^2} \sum_{n=0}^{\infty} n \sin\left(\frac{\pi n}{h} z'\right) \\ &\times \cos\left(\frac{\pi n}{h} z\right) \begin{cases} H_1^{(2)}(k_\rho \rho') J_1(k_\rho \rho), & \rho \leq \rho' \\ J_1(k_\rho \rho') H_1^{(2)}(k_\rho \rho), & \rho \geq \rho' \end{cases}; \end{aligned} \tag{7}$$

Knowledge of H_ϕ magnetic field enables to compute the electric fields E_z, $E\rho$ in the parallel plates as described in [17].

B. MoM Formulation

Evaluation of the current distribution on the conductive probes in the radial line is possible either by numerical solution of a differential equation using methods like finite element method (FEM) or finite difference time domain (FDTD) method or by solving an integral equation using MoM. In the case under consideration the MoM is beneficial because of its small surface to volume ratio, which translates into less memory and computational time, therefore it was the chosen method. The integral equation formulation used in this problem is the electric field integral equation (EFIE) due to its relative simplicity. The requirement of the EFIE formulation is that the total tangential electric fields on the conductive probes surface vanish. This requirement results into two coupled integral equations in the following form:

TABLE I
MoM IMPEDANCE MATRIX ENTRIES

	Case $\mathbf{A} \neq \mathbf{B}$	Case $\mathbf{A} = \mathbf{B}$
Z_{zz}	$-\frac{\pi a}{2h\omega\varepsilon}\sum_{n=0}^{\infty}\varepsilon_n k_\rho^2 \chi_{nm}\chi_{nq} J_0(k_\rho a) H_0^{(2)}(k_\rho \rho_{AB})$	$-\frac{\pi a}{2h\omega\varepsilon}\sum_{n=0}^{\infty}\varepsilon_n k_\rho^2 \chi_{nm}\chi_{nq} J_0(k_\rho a) H_0^{(2)}(k_\rho a)$
$Z_{z\rho}$	$-\frac{\pi^2}{2h^2\omega\varepsilon}\sum_{n=1}^{\infty}k_\rho^2 n \sin(\frac{\pi n}{h} l_B)\chi_{nm} H_0^{(2)}(k_\rho \rho_{AB}) \mathrm{X}_1^q$	$-\frac{\pi^2}{2h^2\omega\varepsilon}\sum_{n=1}^{\infty}k_\rho^2 n \sin(\frac{\pi n}{h} l_A)\chi_{nm} H_0^{(2)}(k_\rho a) \mathrm{X}_1^q$
$Z_{\rho z}$	$-\frac{\pi a}{h\omega\varepsilon}\sum_{n=1}^{\infty}(\frac{\pi n}{h}) k_\rho \sin(\frac{\pi n}{h} l_B)\chi_{nm} J_0(k_\rho a)\Psi_1^q$	$-\frac{\pi a}{h\omega\varepsilon}\sum_{n=1}^{\infty}(\frac{\pi n}{h}) k_\rho \sin(\frac{\pi n}{h} l_A)\chi_{nm} H_0^{(2)}(k_\rho a)\Psi_1^q$
$Z_{\rho\rho}$	$-\frac{\pi^3}{2h^3\omega\varepsilon}\sum_{n=1}^{\infty}n^2 k_\rho \sin(\frac{\pi n}{h} l_B)\cos(\frac{\pi n}{h} l_A)\Psi_3^{mq}$	$-\frac{\pi^3}{2h^3\omega\varepsilon}\sum_{n=1}^{\infty}n^2 k_\rho \sin(\frac{\pi n}{h} l_A)\cos(\frac{\pi n}{h} l_A)\mathrm{X}_1^m \Psi_1^q$

TABLE II
MoM INCIDENT VECTOR ENTRIES

	Case $\mathbf{A} \neq \mathbf{B}$	Case $\mathbf{A} = \mathbf{B}$
V_z^{inc}	$\frac{j\pi}{2h\ln(b/a)}\sum_{n=0}^{\infty}\varepsilon_n \chi_{nm}(J_0(k_\rho b) - J_0(k_\rho a)) H_0^{(2)}(k_\rho \rho_{AB})$	$\frac{jV_0\pi}{2h\ln(b/a)}\sum_{n=0}^{\infty}\varepsilon_n \chi_{nm}(H_0^{(2)}(k_\rho b) - H_0^{(2)}(k_\rho a)) J_0(k_\rho a)$
V_ρ^{inc}	$\frac{j\pi}{h\ln(b/a)}\sum_{n=1}^{\infty}(\frac{\pi n}{h})\sin(\frac{\pi n}{h} l_B)\frac{(J_0(k_\rho b) - J_0(k_\rho a))}{k_\rho}\Psi_1^m$	$\frac{jV_0\pi}{h\ln(b/a)}\sum_{n=1}^{\infty}(\frac{\pi n}{h})\sin(\frac{\pi n}{h} l_A)\frac{(H_0^{(2)}(k_\rho b) - H_0^{(2)}(k_\rho a))}{k_\rho}\Psi_2^m$

$$
\begin{aligned}
E_z^{inc} + E_z^{scat}(J_z) + E_z^{scat}(J_\rho) &= 0 \\
E_\rho^{inc} + E_\rho^{scat}(J_z) + E_\rho^{scat}(J_\rho) &= 0
\end{aligned} \tag{8}
$$

in which E_z^{inc}, E_ρ^{inc} are the z and ρ components of the incident electrical field due to the coaxial cable opening of the central excitation probe and E_z^{scat}, E_ρ^{scat} are the scattered fields from all probes under investigation. The numerical solution of the integral equation is based on MoM using Galerkin formulation with basis and testing functions set as polynomial functions [21], such that the current distribution on the probes, $J_z(z)$ and the radial current distribution on their cap, $J_\rho(\rho)$ can be represented by

$$
J_z(z) = \sum_{m=1}^{M_z} C_m (z - l)^m + C_0 \tag{9}
$$

and

$$
J_\rho(\rho) = \sum_{m=1}^{M_\rho} K_m (\rho - a)^m + C_0. \tag{10}
$$

In the above expressions, a is the probe radius and l is the length of the probe. The coefficient, C_0 guarantees continuity of the current at $z = l$. The MoM formulation results in the matrix equation:

$$
\begin{gathered}
\mathbf{Z}\mathbf{I} = \mathbf{V}_{inc} \\
\Downarrow \\
\left[\begin{array}{c|c} \mathbf{Z}_{zz} & \mathbf{Z}_{z\rho} \\ \mathbf{Z}_{\rho z} & \mathbf{Z}_{\rho\rho} \end{array}\right] \begin{bmatrix} \mathbf{I}_z \\ \mathbf{I}_\rho \end{bmatrix} = \begin{bmatrix} \mathbf{V}_z^{inc} \\ \mathbf{V}_\rho^{inc} \end{bmatrix}
\end{gathered} \tag{11}
$$

in which $[\mathbf{Z}_{zz}]$ is an $(M_z + 1) \times (M_z + 1)$ sub-matrix and $[\mathbf{Z}_{\rho\rho}]$ is an $(M_\rho + 1) \times (M_\rho + 1)$ sub-matrix. $\mathbf{Z}_{ij}$ is a sub-matrix of $\mathbf{Z}$ matrix and, in general, it expresses the relation between the i-component of the scattered field and the j-directed current.

For the sake of completeness, the entries of the above matrices are summarized in Tables I and II. All the expressions in the tables refer to the coupling between the mth-basis function of the current on probe A and qth-basis function of the current on probe B. The distance between the center points of the probes A and B is denoted by ρ_{AB}.

In Tables I and II the following abbreviations were used:

$$
X_1^m \equiv \int_0^a \rho'^2 (\rho' - a)^m d\rho' \tag{12a}
$$

$$
X_2^m(\rho) \equiv \int_0^\rho \rho'^2 (\rho' - a)^m d\rho' \tag{12b}
$$

$$
X_3^m(\rho) \equiv \int_\rho^a \rho'^2 (\rho' - a)^m d\rho' \tag{12c}
$$

$$
\chi_{nm} \equiv \int_0^l (z' - l)^m \sin\left(\frac{\pi n}{h} z'\right) dz' \tag{12d}
$$

$$
\Psi_1^m \equiv \int_0^a H_1^{(2)}(k_\rho \rho')(\rho' - a)^m d\rho' \tag{12e}
$$

$$
\Psi_2^m \equiv \int_0^a J_1(k_\rho \rho')(\rho' - a)^m d\rho' \tag{12f}
$$

$$
\begin{aligned}
\Psi_3^{mq} \equiv \int_0^a (\rho' - a)^m \Bigg(& H_1^{(2)}(k_\rho \rho') X_2^q(\rho') + \left(1 + \frac{j}{\pi}\right) J_1 \\
& \times (k_\rho \rho') \mathrm{X}_3^q(\rho') \Bigg) d\rho'
\end{aligned} \tag{12g}
$$

In the above expressions (12a)–(12d) are evaluated analytically, and (12e)–(12g) are evaluated numerically.

If the $\mathbf{Z}$-matrix is non-singular then its inverse exists and the unknown coefficients of the impressed currents can be found by $\mathbf{I} = \mathbf{Z}^{-1}\mathbf{V}_{inc}$. The size of the $\mathbf{Z}$-matrix is proportional to the number of probes $N+1$ multiplied by the number of basis functions, M describing the unknown currents $M = M_z + M_\rho + 2$, in which M_z and M_ρ represent the number of basis functions used to represent the z and ρ currents on the probes, respectively. Therefore, the number of operations required to compute the matrix $\mathbf{Z}$ is proportional to $O((M(N+1))^2)$. In addition, the number of operations required to invert the $\mathbf{Z}$ matrix is proportional to $O((M(N+1))^3)$. Accordingly, the total computational complexity can be estimated by $O(MoM) = O((M(N+1))^2) + O((M(N+1))^3)$. The number of computations in the case of the RLPA is governed mainly by the second term therefore, $O(MoM) \approx O((M(N+1))^3)$. This term becomes prohibitive in terms of required memory and computation time for medium and large arrays.

III. Design Methodology

In this study, an alternative approach to the inversion of the entire $\mathbf{Z}$ matrix is proposed. The approach is based on the physical assumption that the current distribution on each conductive probe is mainly determined by its close K neighbors enclosed in a circle with a radius of λ around the probe under consideration and the rest of the interactions can be neglected. Accordingly, to evaluate the current distribution of a certain conductive probe, a reduced sized Z matrix with only $MK \times MK$ elements is needed. Thus, the computational time required to compute all the currents could be estimated by $O((N+1)(MK)^2) + O((N+1)(MK)^3) \approx O((N+1)(MK)^3)$ in which the first term refers to the number of operations required to compute the elements of all $\mathbf{Z}$ matrices and the second term refers to the number of operations required to invert all the $\mathbf{Z}$ matrices. This result indicates that the solution using the proposed approach is especially significant in the case of antennas with medium and large number of probes $(K \ll N)$.

Once the currents are known, the self and mutual impedances at the ports $(z = 0)$ of the probes can be determined using the EMF method [18]

$$Z^f_{mn} = -\frac{1}{I_m(0)I_n(0)} \int_0^{l_n} E_z(m, n|z')I_n(z')dz' \tag{13}$$

in which $E_z(m, n \mid z')$ is the electric field at the location of the mth probe due to the radiation of the nth probe with all other probes open circuited. The size of the probes port impedance matrix, $\mathbf{Z}^f$ is $(N+1) \times (N+1)$. The electric field $E_z(m, n|z')$ is composed from the summation of the incident field from the nth probe and the scattered fields from its K neighbors, making the same assumption discussed above. Evaluation of the scattered fields requires the computation of the induced currents on the K open circuit probe neighbors of the mth probe, which are illuminated by the incident field of the nth probe. Therefore, the computational complexity required to compute the $(N+1)^2$ elements of the port impedance matrix Z is equal to $O(MoM) \approx O((N+1)(MK)^3) + O((N+1)^2(MK)^3) \approx O((N+1)^2(MK)^3)$. Additional savings in the computational complexity can be obtained if one recognizes that the RLPA under consideration is composed of concentric circles with $6n$ probes in the nth circle. Thus, the whole antenna can be built by rotating a 60^0 sector. Such a "representing sector" is shown in Fig. 5. One can observe that the port's mutual impedance Z_{ij} between probes i and j (i, j are not located in the "representing" sector) can be mapped to a mutual impedance between probes k and l, such that probe i corresponds to probe k in the "representing" sector and probe j is mapped to probe l which its relative position to k is identical to the position of j relative to i. This mapping reduces the amount of impedance matrix entries computations from $(N+1)^2$ to $(N+1)^2/6$.

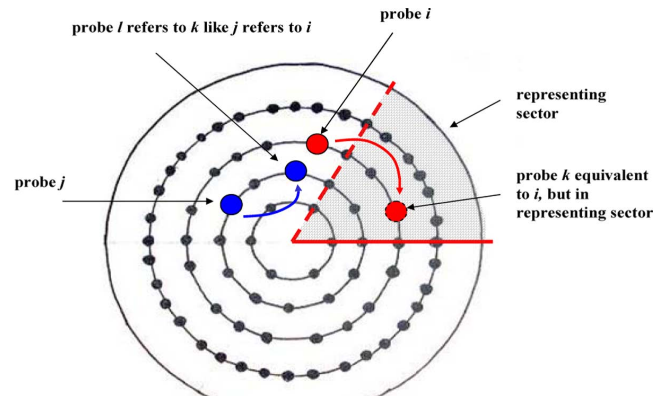

Fig. 5. The representing sector of the RLPA.

Two additional savings each by a factor of 2, are related to the filling of the port impedance matrix $\boldsymbol{Z}^f$. The first is related to the reciprocity of the $\boldsymbol{Z}^f$ matrix elements such that $Z^f_{ij} = Z^f_{ji}$. The second is related to the observation that if probes i and j make an angle of $\Delta\phi(i, j)$ between them, exists an additional probe k, which makes a negative angle with probe j and is related to j in the same fashion as the probes j and i are related, such that $Z^f_{ij} = Z^f_{kj}$. These two type of savings reduce the total computation complexity of the proposed MoM approach to $O(MoM) \approx O(((N+1)^2(MK)^3)/24)$ in comparison to $O((N+1)^2(M(N+1)^3)$ using the straightforward matrix filling.

Initially, the necessity to take in consideration the radial currents on the probes cap for the simulation accuracy was tested. Fig. 6 shows the improvement in the accuracy of the self impedance of a long probe due to the addition of the radial currents contribution by comparing three models: the CST simulation, the MoM results without radial currents and the MoM results with the added radial currents. The probe length is $l = 8$ mm, its radius is $a = 0.255$ mm and the height of the radial line is $h = 9$ mm. As it can be noticed, the addition of the radial current contribution significantly improves the accuracy of the self impedance values. For smaller size probes, the contribution of the radial currents on the probe cap is less significant and can be neglected.

A computational time comparison between CST and the proposed MoM procedure of the port impedance matrix, $\mathbf{Z}^f$ for various cases, is shown in Table III. The computations were performed on a PC with a 2 Xeon Quad core processor with 16 GB

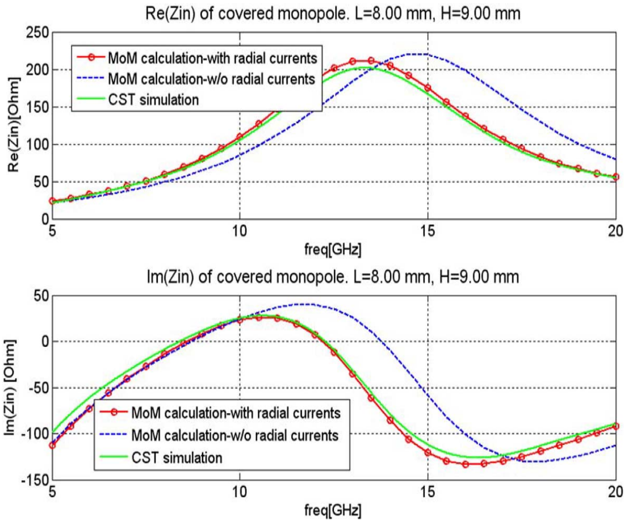

Fig. 6. Real and imaginary self input impedance of a single probe in the radial line ($l = 8$ mm, $h = 9$ mm, $a = 0.255$ mm).

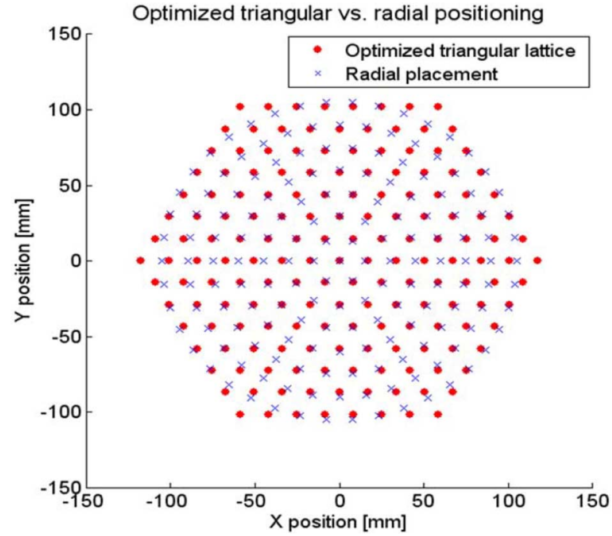

Fig. 7. Comparison between a 7 circles circular array configuration to an optimized equilateral triangular grid lattice.

TABLE III
COMPUTATION TIME FOR DIFFERENT CASES OF THE PORT IMPEDANCE MATRIX, $\mathbf{Z}^f$.

Setup	CST time [min]	MoM time [min]
1 circle (4 probes)	~20	~1
1 circle (7 probes)	~65	~1.5
2 circles (19 probes)	~380	~8
7 circles (169 probes)	~150*	~40

*-this time refers to the simulation of only one port.

RAM. The meshing in the CST simulations was $\lambda_H/15$ and in the MoM simulations, 40 parallel modes and 4 basis functions were used.

The results confirm the efficiency of the proposed MoM. Time savings with a ratio of 1:47 are obtained for an antenna with 19 probes. This saving ratio increases with the size of the antenna as explained above.

The active impedance of the radiating element determines the port impedance of each probe in the array. Computation of the active impedance takes in consideration the external mutual coupling from the element's neighbors.

This type of computation for all the probes is a very tedious process and depends largely on the geometrical complexity of the radiating elements layout.

In this study, a different and more efficient approach to the active impedance computation has been adopted. Close inspection of the array layout reveals that it resembles to a certain extent the layout of an infinite array with an equilateral triangular lattice grid. In such an infinite array, all its elements have identical active impedance and it can be computed using the "unit cell" concept. The computational savings and the accuracy of this assumption increases with the size of the array. The geometrical equilateral triangular grid parameters have been optimized to be very "close" to the original geometrical configuration. Fig. 7, shows such an example of an optimized triangular grid lattice compared to the RLPA layout with seven circles. The two grid layouts are very close, an observation, which justifies the "unit cell" active impedance approach for the array under investigation. Moreover, this assumption is further justified for uniform amplitude distribution of the radiating elements, as is the case in our study.

IV. DESIGN EXAMPLE

The design methodology proposed was implemented for a typical RLPA case of seven circles array with a total number of 168 radiating elements and uniform aperture distribution. The chosen height of the radial line was $h = 7$ mm to allow only propagation of the TEM mode in the radial line in the required frequency band 11.5–12.5 GHz. The spacing between adjacent probes on each circle is $S_{\text{cir}} = 15.7$ mm and the spacing between circles is $S_{rad} = 15$ mm. The radius of all probes is set equal to $a = 0.255$ mm and the feeding coax dimensions of the central excitation probe are: inner radius $a = 0.255$ mm and outer radius $b = 0.586$ mm.

Fig. 8 shows a comparison between the active reflection coefficient of a stand-alone radiating element, the center element in the finite array layout (with all elements excited) and the unit cell element in an infinite array with equilateral triangular lattice grid.

One can observe a satisfactory agreement between the active reflection coefficient of the center element in the finite array and that of the unit cell element in the infinite array. The simulations were performed with the CST commercial software.

In the next phase of the study, the results obtained from the MoM calculations of the radial line feeding network and the active impedance calculations were combined. Given the $\mathbf{Z}^f$-matrix, one can derive the $\mathbf{S}^f$-matrix of the system through the relationship [19]: $\mathbf{S}^f = (\mathbf{Z}^f - \mathbf{Z}_0)(\mathbf{Z}^f + \mathbf{Z}_0)^{-1}$ where $\mathbf{Z}_0$ is a $(N+1) \times (N+1)$ diagonal matrix with $Z_0(i,j)$ equal to the characteristic impedance of port i, usually 50 Ω. In case the active impedance Z_i^a is connected to the port instead of $Z_0(i,j)$, the incident and reflected waves at port i change. The new scattering matrix $\mathbf{S}^{fn}$ connecting these new power vectors is different from the original one.

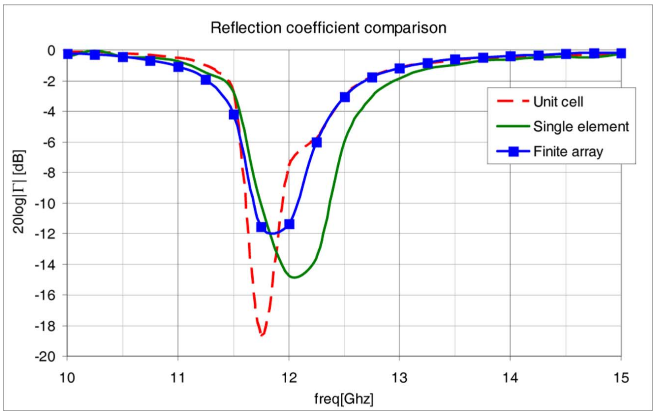

Fig. 8. Reflection coefficient comparison between the stand-alone radiating element, the active reflection coefficient of the center element in the finite array and the active reflection coefficient of the unit cell element in an equilateral triangular grid lattice infinite array.

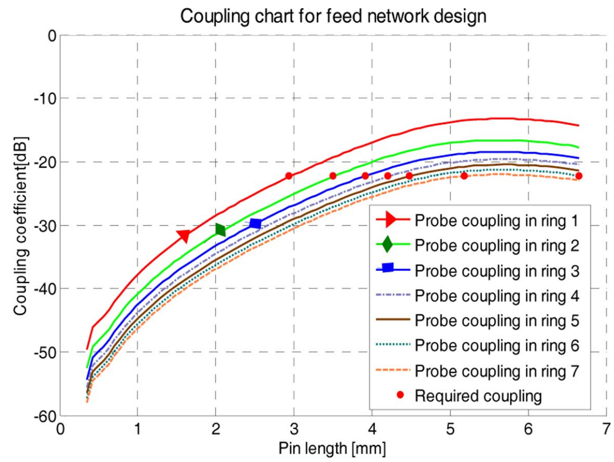

Fig. 9. Coupling vs. probe length on different circles based on the procedure described in [10].

However, it is expressible in terms of the original $\mathbf{S}^f$ and the power wave reflection coefficient r_i of Z_i^a with respect to $Z_0(i,i)$ [20], i.e.,

$$\mathbf{S}^{fn} = \mathbf{A}^{-1}(\mathbf{S}^f - \mathbf{\Gamma}^H)(\mathbf{U} - \mathbf{\Gamma}\boldsymbol{S}^f)^{-1}\mathbf{A}^H \tag{14}$$

in which $\mathbf{\Gamma}$ and $\mathbf{A}$ are diagonal matrices with their ith diagonal components being r_i and $(1-r_i^*)\sqrt{1-|r_i|^2}/|1-r_i|$, respectively. In (11), $(\ )^{\mathrm{H}}$ indicates the complex conjugate transposed matrix. The reflection coefficient, r_i is given by $r_i = (Z_i^a - Z_0(i,i))\,/\,(Z_i^a + Z_0(i,i))$. In this way the scattering matrix S^f of the feeding network and the active impedance Z_i^a of the radiating element are combined to represent the performance of the entire system (feeding network and radiating elements).

The radiating element used in the simulations is a microstrip circular patch. In the patch metallization, there are two indents, which are optimized to give circular polarization. The necessary feature of the proposed element is its capability to control the phase of the radiated field by turning the radiating patch around its feeding probe. This is a desirable feature for this type of antenna because it enables to correct the phase of the radiated fields on each circle. CST simulations of the stand-alone patch provide the rotation angle of the elements in a certain circle in the same manner as discussed in [12].

Using the procedure outlined in [10] the plots in Fig. 9 were generated and have been used to determine the initial values of the probes. Table IV outlines the required probes coupling coefficients to obtain uniform distribution, the initial probes lengths extracted from Fig. 9, the corresponding coupling coefficients computed with the proposed MoM procedure, the final probe lengths after an iterative optimization process and the corresponding computed coupling coefficients for these probe lengths.

The length of the central excitation probe is 5.65 mm and was obtained from the requirement of matching considerations of the RLPA at the design frequency. Fig. 10 shows the dependence of the coupling coefficient of various probes on the third circle.

The comparison is made between CST and MoM results for several frequencies. One can observe a fluctuation in the coupling coefficients for different probes. This fluctuation is due to a “shadowing” effect to the incident wave caused by probes on smaller radius circles.

This interesting effect has been observed experimentally in [3] and validated numerically in this study. Fig. 11 shows the feeding network reflection coefficient at the feeding network

TABLE IV
COUPLING AND PROBE LENGTHS AT THE INITIAL AND FINAL STAGES OF THE DESIGN

Circle #	1	2	3	4	5	6	7
req. coup. [dB]	-22.3	-22.3	-22.3	-22.3	-22.3	-22.3	-22.3
init. coup. [dB]	-21.7	-25	-21	-20	-21	-19.1	-26.5
init. length [mm]	2.9	3.5	3.9	4.2	4.5	6.6	5.2
final coup. [dB]	-22.3	-23.5	-22.7	-20.5	-21.6	-21.7	-26
final length [mm]	2.9	3.8	4.2	4.3	4.5	6.5	6.6

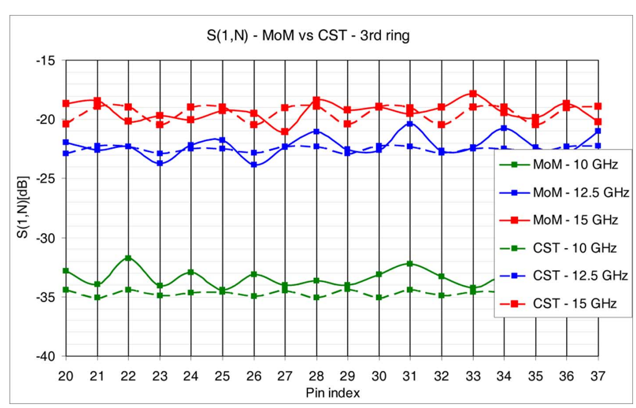

Fig. 10. Comparison between CST and MoM results for the coupling coefficient on the third circle as a function of the probe index for different frequencies.

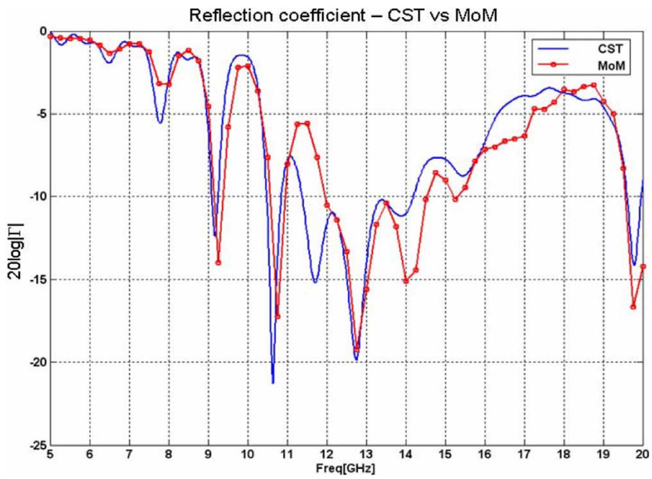

Fig. 11. Comparison between CST and MoM results for the reflection coefficient at the input central probe of the seven circle feeding network.

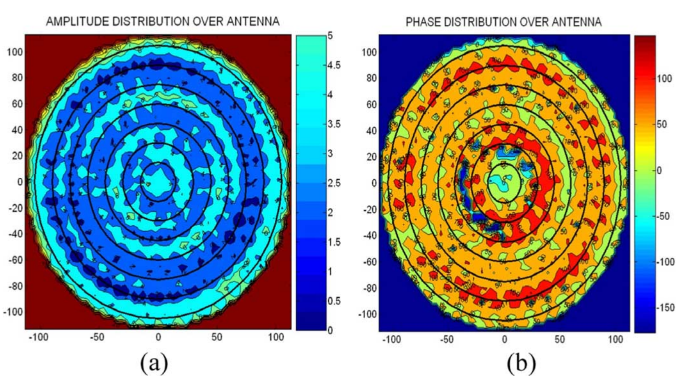

Fig. 12. Near field distribution (a) amplitude and (b) phase above the simulated antenna at 12 GHz.

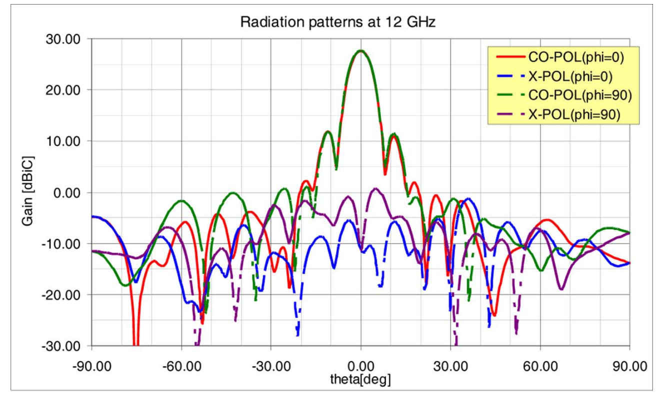

Fig. 13. RLPA radiation patterns (co-pol and x-pol components) at 12 GHz in two cardinal planes ($\phi = 0^0, \phi = 90^0$).

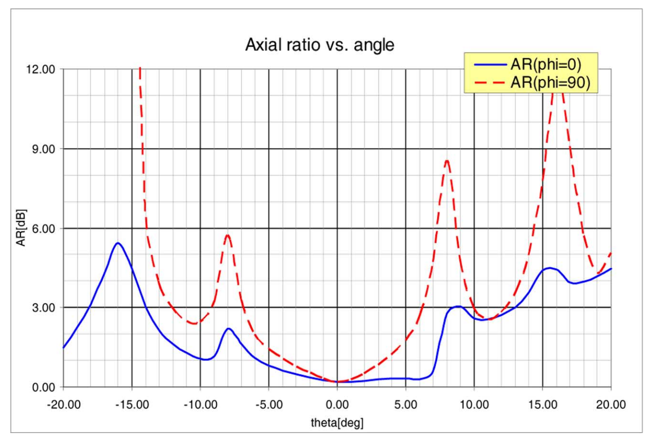

Fig. 14. Axial ratio at 12 GHz in two cardinal planes ($\phi = 0^0, \phi = 90^0$).

input. The final antenna comprising of the feeding network and the optimized radiating element was simulated with CST commercial software. Fig. 12 shows the simulated near-field phase and amplitude distribution at 12 GHz at a distance 0.2λ above the aperture. The black rings denote the array element rings location.

The amplitude distribution shows the absolute value of the field strength and the phase distribution shows the phase difference of the two orthogonal field components relative to 90^0.

One can observe the uniformity of the phase and amplitude distribution. Figs. 13 and 14 show the radiation patterns (copol and xpol) and the axial ratio of the RLPA obtained at 12 GHz in the two cardinal planes ($\phi = 0^0, 90^0$). The axial ratio on the antenna boresight is less then 1 dB. The antenna aperture efficiency is 82%.

The results show a good agreement with the theoretical predictions, which in turn demonstrates the accuracy of the proposed design methodology.

V. Conclusion

An efficient full wave analysis and a new design methodology for the RLPA was presented. The analysis of the feeding network is based on MoM solution of EFIE formulation with corresponding Green's functions. It has been demonstrated that taking in consideration the radial currents on the probes cap is significant for long probes. Assumptions made on the minimum radius size of the coupling neighborhood for the feeding conductive probes in the radial line enabled significant time reduction of the computational time spent on the matrix inversion. Explorations of the RLPA symmetries lead to a considerable simplification to the computation and the filling process of the port impedance matrix. The MoM results of the feeding network were combined with the results of the radiating elements for obtaining the performance of the entire antenna taking in consideration the external (outside the radial line) coupling by approximating the array lattice by an equilateral triangular lattice of an infinite array. Finally, a seven circles antenna array with 168 radiating elements with uniform aperture distribution operating at 12 GHz was designed. Comparison of the computational time using the proposed MoM formalism and CST show significant savings and the computed results are found to be in a good agreement.

References

[1] F. J. Goebels and K. C. Kelly, "Arbitrary polarization from annular slot planar antennas," *IRE Trans. Antennas Propag.*, vol. 4, pp. 342–349, Jul. 1961.

[2] K. R. Carver, "A Cavity-Fed Concentric Ring Phased Array of Helices for Use in Radio Astronomy," Ph.D. dissertation, Ohio State Univ., Columbus, 1967.

[3] H. Nakano, H. Takeda, Y. Kitamura, H. Mimaki, and J. Yamauchi, "Low profile helical array antenna fed from a radial waveguide," *IEEE Trans Antennas Propag.*, vol. 3, pp. 79–284, Mar. 1992.
[4] M. Haneishi and S. Saito, "Radiation properties of microstrip array antenna fed by radial line," in *IEEE Antennas Propag. Symp. Dig.*, 1991, pp. 588–591.
[5] N. Yamamoto, S. Saito, S. Morishita, and M. Haneishi, "Radiation properties of shaped beam antenna using radial line microstrip array," in *IEEE Antennas Propag. Symp. Dig.*, 1996, pp. 1924–1927.
[6] H. Miyashita and T. Katagi, "Radial line planar monopulse antenna," *IEEE Trans. Antennas Propag.*, vol. 8, pp. 1158–1165, Aug. 1996.
[7] N. Takemura, H. Myashita, and S. Makino, "Wave analysis of the aperture field distribution in probe-fed radial line planar antennas," *IEICE Trans. Commun.*, vol. E89-B, no. 9, pp. 2580–2586, Sep. 2006.
[8] L. Pazin and Y. Leviatan, "Uniform amplitude excitation of radiating elements in array antenna pin-fed from a radial waveguide," *IEE Proc. Microw. Antennas Propag.*, vol. 148, no. 6, pp. 413–417, Dec. 2001.
[9] L. Pazin and Y. Leviatan, "Effect of amplitude tapering and frequency dependent phase errors on radiating characteristics of radial waveguide fed nonresonant array antenna," *IEE Proc. Microw. Antennas Propag.*, vol. 151, no. 4, pp. 363–369, Aug. 2004.
[10] L. Pazin and Y. Leviatan, "Design of a radial waveguide feed network for a pin-fed array antenna," *IEE Proc. Microw. Antennas Propag.*, vol. 153, no. 1, pp. 38–42, Feb. 2006.
[11] R. Shavit, L. Pazin, Y. Israeli, M. Sigalov, and Y. Leviatan, "Dual frequency and dual polarization microstrip nonresonant array pin-fed from a radial line," *IEEE Trans. Antennas Propag.*, vol. 53, no. 12, pp. 3897–3905, Dec. 2005.
[12] R. Shavit, Y. Israeli, L. Pazin, and Y. Leviatan, "Dual frequency circularly polarized microstrip antenna," *IEE Proc. Microw. Antennas Propag.*, vol. 152, no. 4, pp. 267–272, Aug. 2005.
[13] M. E. Bialkowski and P. Kabacik, "An electromagnetic-field method modeling of a radial line planar antenna with coupling probes," *IEEE Trans. Antennas Propag.*, vol. 51, no. 5, pp. 1114–1120, May 2003.
[14] M. Albani, A. Freni, and R. Gardelli, "An efficient full-wave method of moments analysis for RLSA antennas," *IEEE Trans. Antennas Propag.*, vol. 54, no. 8, pp. 2326–2336, Aug. 2006.
[15] M. Abramowitz and I. A. Stegun, *Handbook of Mathematical Functions*, 9th ed. Dover, New York: , 1972.
[16] B. Tomasic and A. Hessel, "Electric and magnetic current sources in the parallel plate waveguide," *IEEE Trans. Antennas Propag.*, vol. 35, no. 11, pp. 1307–1310, Nov. 1987.
[17] R. F. Harrington, *Time-Harmonic Electromagnetic Fields*. New York: McGraw-Hill, 1961.
[18] R. S. Elliott, *Antenna Theory and Design*. Englewood Cliffs, NJ: Prentice-Hall, 1981.
[19] D. M. Pozar, *Microwave Engineering*, 2nd ed. New York: Wiley, 1998.
[20] K. Kurokawa, "Power waves and the scattering matrix," *IEEE Trans. Microwave Theory Tech.*, vol. 13, no. 2, pp. 194–202, Mar. 1965.
[21] B. D. Popovic, M. B. Dragovic, and A. R. djordjevic, *Analysis and Synthesis of Wire Antennas*. New York: Wiley, 1982.

Oleg Becker (S'09) was born in Ukraine on February 2, 1979. He received the B.Sc. degree in electrical engineering from the Technion-Israel Institute of Technology, Haifa, Israel, in 2002 and the M.Sc. degree from Ben-Gurion University of the Negev, Beer-Sheva, Israel.

During his undergraduate studies he worked as a Staff Engineer in the MRC company, Haifa, where he was involved in system on chip design. He was also involved in the design of active and passive microwave devices. Currently, he is associated with the Israeli Aircraft Industries working as Antenna Engineer. His present research interest is in the area of efficient numerical methods for antenna design.

Reuven Shavit (M'82–SM'90) was born in Rumania on November 14, 1949. He received the B.Sc. and M.Sc. degrees in electrical engineering from the Technion-Israel Institute of Technology, Haifa, Israel, in 1971 and 1977, respectively, and the Ph.D. degree in electrical engineering from the University of California, Los Angeles, in 1982.

From 1971 to 1993, he worked as a Staff Engineer and Antenna Group Leader in the Electronic Research Laboratories of the Israeli Ministry of Defense, Tel Aviv, where he was involved in the design of reflector, microstrip, and slot antenna arrays. He was also a part-time lecturer at Tel Aviv University, teaching various antenna and electromagnetic courses. From 1988–1990 he was associated with ESSCO, Concord, MA, as a Principal Engineer involved in scattering analysis and tuning techniques of high performance ground based radomes. Currently, he is with Ben-Gurion University of the Negev, as an Associate Professor doing research in microwave components and antennas. His present research interest is in the areas of smart antennas, tuning techniques for radomes and numerical methods for design microstrip, slot and reflector antennas.